Solvent- and Tatrz-Induced Single-Crystal-to-Single-Crystal Transformations within Cobalt(II)-Triazole MOFs: a Luminescent Probe for Frankincense

Jialin Feng,[#,a] Jianshuai Mu,[#,*,a] Zhengyu Liu,[#,a] Lin Cheng,[*,a] Siyu Li,[a] Xin Cheng,[a] Shaowei Zhang,[*,b] Xin Meng,[a] and Ying Wang*[,a]

[a.]College of Chemistry, Tianjin Normal University, Tianjin 300387, P.R. China; Email: hxxywy@tjnu.edu.cn; hxxycl@tjnu.edu.cn; hxxymujianshuai@tjnu.edu.cn.

[b.]School of Chemistry and Chemical Engineering, Key Laboratory of Theoretical Organic Chemistry and Functional Molecule of the Ministry of Education, Hunan University of Science and Technology, Xiangtan, Hunan 411201, China. Email: swzhang@hnust.edu.cn.

Supporting Information:

Experimental Section

General remarks: All the reagents were commercially available and used without further purification. The C, H, and N elemental analysis was conducted on a Perkin-Elmer 240 elemental anaoyzer. Powder X-ray diffraction measurement was recorded on a D/Max-2500 X-ray diffractometer using Cu *K*α radiation. ^{1}H NMR data were collected using a Bruker Avance 400 MHz spectrometer. Chemical shifts are reported in δ relative to TMS (TMS = tetramethylsilane). The photoluminescence spectrum was measured by Edinburgh Instruments FLS1000 spectrophotometer with a xenon arc lamp as the light source. The UV-vis absorption spectra were recorded on a HITACHI U-4100 spectrophotometer. FT-IR spectra were recorded from KBr pellets in the range 4000-400 cm^{-1} on a Nicolet IR-200. The N_2 adsorption-desorption isotherms were measured on an ASAP 2020 Physisorption Analyzer (Micromeritics, USA) at 77 K.

Synthesis of 1-(9-(1H-1,2,4-triazol-1-yl)anthracene-10-yl)-1H-1,2,4-triazole (tatrz)

9,10-dibromoanthracene was synthesized by procedures reported earlier.[S1] A mixture of 9,10-dibromoanthracene (0.92 g, 2.74 mmol), 1H-1,2,4-triazole (0.38 g, 5.48 mmol),

potassium carbonate (0.76 g, 5.48 mmol) and CuO (0.01 g, 0.125mmol) were heated while stirring in 15 mL of DMSO at 150 ºC for 48 h. The resulting slurry was cooled to room temperature, and solids were removed by filtration. DMSO of the filtrate was removed by distillation under reduced pressure. Methylene chloride was added to the remaining filtrate, and the mixture was then washed with water and dried over sodium sulfate. The methylene chloride was then removed. The products were crystallized in methanol and water, and deep yellow solids were obtained.

Synthesis of $\{[Co(tatrz)(ipa)]\cdot H_2O\}_n$ (1)

A mixture of tatrz (0.0234 g, 0.075 mmol), $Co(NO_3)_2\cdot 6H_2O$ (0.0218 g, 0.075 mmol), ipa (0.0125 g, 0.075 mmol) and H_2O (6 mL) were put in a 20 mL acid-digestion bomb and heated at 90 °C for 3 days. The reddish-brown block crystals suitable for single-crystal X-ray diffraction experiments were collected after washing with H_2O (2 × 5 mL) and diethyl ether (2 × 5 mL). Yield: 65%. Elemental analysis calcd (%) for $C_{28.5}H_{21.5}CoN_{6.5}O_{4.5}$: C 58.42, H 3.70, N 15.54; found: C 58.33, H 3.79, N 15.62.

Synthesis of $\{[Co(tatrz)(ipa)]\cdot DMF\}_n$ (2)

100 mg proper size crystals of **1** were soaked in DMF (10 mL) for 6 h. The resulting rufous crystals suitable for single-crystal X-ray diffraction studies were separated from DMF and were thoroughly washed with diethyl ether (2 × 5 mL). Elemental analysis calcd (%) for $C_{58}H_{46}Co_2N_{14}O_{10}$: C 57.24, H 3.81, N 16.11; found: C 57.16, H 3.92, N 16.19.

Synthesis of $\{[Co(tatrz)(ipa)(H_2O)]\cdot(tatrz)_{0.5}\}_n$ (3)

100 mg proper size crystals of **1** were soaked in an ethanol solution of tatrz (0.3 g) for 3 days. The resulting flesh pink crystals suitable for single-crsytal X-ray diffraction studies were separated and thoroughly washed by diethyl ether (2 × 5 mL). Elemental analysis calcd (%) for $C_{35}H_{24}CoN_9O_5$: C 59.25, H 3.41, N 17.77; found: C 59.16, H 3.46, N 17.82.

Thermal Stability

The thermogravimetric analysis (TGA) curves (Figs. S3†-S5†) show that a 2.91% weight loss for **1** (theoretical 3.07%), a 12.01% weight loss for **2** (theoretical 12.15%), and a 2.42% weight loss for **3** (theoretical 2.54%) in the temperature ranges of 25-138 °C, 25-281 °C, and 25-105 °C, respectively. These results are consistent with the removing of lattice water molecules in **1**, DMF in **2** and

coordination water molecules in **3**. It is noted that guest tatrz moieties could be completely removed in temperatures ranging from 106 to 366 °C (calcd: 42.04%, obsd: 41.76%). Above 400 °C, the frameworks of MOFs **1** - **3** collapse because the organic ligands have been decomposed.

PXRD Results

PXRD spectra determined for the crystal materials of MOFs **1** - **3** and their calculated patterns deduced from single-crystal X-ray data are highly consistent, not only in respect of the sharpness of the lines but also the position of the peaks (Figs. S6†-S8†). The result reveals that single-crystal structures are representative of the bulk of the corresponding samples. The differences in reflection intensities between the experimental and the simulated patterns are due to the variations in the crystal orientation of the powder samples.

Luminescent properties

To quantitatively assess the quenching efficiency, the Stern-Volmer (S-V) equation was employed, $I_0/I - 1 = K_{SV}[M]$,[S2] in which K_{SV} is the S-V constant ($L \cdot mol^{-1}$), [M] is the concentration of analyte ($mmol \cdot L^{-1}$), I_0 and I represent the maximum emission intensities before and after adding analyte, respectively. However, the S-V curve significantly deviates from linearity, which might be mainly ascribed to the presence of the competitive absorption mechanism.[S3] Therefore, the exponential S-V equation was used to evaluate the full concentration range, $I_0/I = a*\exp(k[M]) + b$,[S3] in which a, b and k are constants, [M] is the concentration of analyte ($mmol \cdot L^{-1}$), I_0 and I are the maximum emission intensities before and after adding analyte, respectively, The results indicate that the entire concentration range could be well fitted by the equation $I_0/I = 2.541*\exp(1.403[M]) - 1.427$ (Fig. S10†), and the K_{SV} value of frankincense is calculated to be 3.565×10^3 $L \cdot mol^{-1}$ based on the fitting constants of a and k.

FT-IR characterizations

In the FT-IR spectra of MOF **1**-**3** (Figs. S11†-S13†), the peak at about 1700 cm^{-1} is assigned to the bond in between Co atom and carboxylic groups (O-C=O) of isophthalic acid. The peaks in the range of 1600-1400 cm^{-1} are assigned to the anthracene ring

skeleton. The broad band at ca. 3400 cm^{-1} in Fig. S13† should be correlated with coordinated water molecules in MOF **3**. While comparatively weaker band at about 3450 cm^{-1} in Fig. S11† can be assigned to dissociative water molecules in MOF **1**. The vibration bands around ca 830 cm^{-1} can be ascribed to the presence of aromatic benzene rings in MOF **1-3**. The triazole out of plane ring absorption can be observed at around 630 cm^{-1}.[S4]

Porosity of MOF 1

MOF **1** has been activated at ca. 150 ^{o}C under high vacuum before N_2 isotherm at 77 K. The powder X-ray diffraction pattern of active MOF **1** before N_2 adsorption at 77 K has been shown in Fig. S6†. BJH adsorption cumulative volume of pores between 1.7 nm and 300 nm width is 0.014285 cm^3/g. BET surface area and Langmuir surface area in MOF **1** is 9.7 m^2/g and 14.4 m^2/g, respectively.

UV-vis spectra

All UV-vis absorption spectra of MOFs **1-3** and tatrz in the solid state were recorded at room temperature (Fig. S16†). Two characteristic absorption peaks of anthracene in tatrz are 280 and 381 nm, respectively, due to the K-band and B-band appeared separately.[S5] Both of the K-band and B-band correspond to the $\pi \rightarrow \pi^*$ transitions.[S6] The absorption band profiles of the characteristic K-band (I: K-band region of ca. 200-280 nm) and B-band (II: B-band region of ca. 340-420 nm) for MOF **1-3** are still typical, which are a little bit red-shifted as compared to those absorption maxima of tatrz ligands.[S5] Therefore, the results show that the characteristic K-band and B-band absorption in the UV-vis spectra of MOF **1-3** should be mainly assigned to $\pi \rightarrow \pi^*$ transitions of tatrz.

References

[S1] S. Jones, J. C. C. Atherton, An improved procedure for the preparation of 9,10-dibromoanthracene, *Synth. Commun.*, 2001, **31**, 1799-1802.

[S2] Y. Xie, S. Ning, Y. Zhang, Z. Tang, S. Zhang and R. Tang, A 3D supramolecular network as highly selective and sensitive luminescent sensor for PO_4^{3-} and Cu^{2+} ions in aqueous media, *Dyes Pigm.*, 2018, **150**, 36-43.

[S3] (a) Z. Tang, H. Chen, Y. Zhang, B. Zheng, S. Zhang and P. Cheng, Functional Two-Dimensional Coordination Polymer Exhibiting Luminescence Detection of Nitroaromatics, *Cryst. Growth Des.*, 2019, **19**, 1172-1182; (b) S. Ning, B. Yan, J. Wu, S. Chen, W. Chen, H. Tian and S. Zhang, A stable 2D

luminescent metal–organic framework as a highly sensitive sensor for Fe^{3+} and $Cr_2O_7^{2-}/CrO_4^{2-}$ in water, *CrystEngComm*, 2023, **25**, 3539-3547.

[S4] (a) J. A. Wolny, S. Rackwitz, K. Achterhold, Y. Garcia, K. Muffler, A. D. Naik, V. Schünemann, Vibrational properties of the trinuclear spin crossover complex $[Fe_3(4\text{-}(2'\text{-hydroxy-ethyl})\text{-}1,2,4\text{-triazole})_6(H_2O)_6](CF_3SO_3)_6$: a nuclear inelastic scattering, IR, Raman and DFT study, *Phys. Chem. Chem. Phys.*, 2010, **12**, 14782-14788; (b) Z. Fan, Y. Y. Wang, Y. Y. Xu, X. M. Su, X. X. Wu, J. Z. Huo, B. Ding, Y. Wang, J. H. Guo, Synthesis and characterization of a novel 3D porous luminescent Ag(I) framework with a multidentate triazole ligand, *Inorg. Chim. Acta*, 2014, **410**, 178-182.

[S5] J.-J. Wang, C.-S. Liu, T.-L. Hu, Z. Chang, C.-Y. Li, L.-F. Yan, P.-Q. Chen, X.-H. Bu, Q. Wu, L.-J. Zhao, Z. Wang and X.-Z. Zhang, Zinc(II) coordination architectures with two bulky anthracene-based carboxylic ligands: crystal structures and luminescent properties, *CrystEngComm*, 2008, **10**, 681-692.

[S6] (a) J. F. Ma, J. Yang, S. L. Li, S.-Y. Song, Two Coordination Polymers of Ag(I) with 5-Sulfosalicylic Acid, *Cryst. Growth Des.*, 2005, **5**, 807-812, and references therein; (b) S. Q. Liu, T. Kuroda-Sowa, H. Konaka, Y. Suenaga, M. Maekawa, T. Mizutani, G. L. Ning, M. Munakata, Silver(I) Coordination Polymers of Fluorescent Oligo(phenylenevinylene) with π-π Stackings: Luminescence and Conductivity, *Inorg. Chem.*, 2005, **44**, 1031-1036.

Table S1. Crystallographic Data and Details of Refinements for MOFs **1**-**3**.

	1	**2**	**3**
formula	$C_{28.50}H_{21.50}CoN_{6.50}O_{4.50}$	$C_{58}H_{46}Co_2N_{14}O_{10}$	$C_{35}H_{24}CoN_9O_5$
M (g mol^{-1})	585.95	1216.95	709.56
crystal system	Triclinic	Triclinic	Triclinic
space group	P-1	P-1	P-1
temperature	296(2)	296(2)	296(2)
a (Å)	10.1722(11)	10.1872(8)	10.242(7)
b (Å)	11.4638(13)	11.7035(9)	12.786(8)
c (Å)	13.3885(16)	13.0008(10)	13.807(9)
α (º)	112.942(2)	113.5490(10)	63.824(12)
β (º)	112.305(2)	110.3460(10)	70.563(13)
γ (º)	90.803(2)	90.9320(10)	79.963(13)
V (Å^3)	1305.9(3)	1310.40(18)	1529.4(17)
Z	2	1	2
F (000)	602	626	728
ρ_{calc} (Mg m^{-3})	1.490	1.542	1.541
μ (mm^{-1})	0.708	0.711	0.623
data/restraints/params	5402 / 0 / 334	5422 / 0 / 381	6333 / 0 / 451
GOF on F^2	1.076	1.047	1.007
R_1[a] (I=2σ(I))	0.0367	0.0372	0.0731
ωR_2[a] (all data)	0.0899	0.1031	0.1902

Table S2. Selected bond lengths [Å] and angles [º] for MOFs **1** - **3**.

1					
Co(1)-O(3)#1	2.0232(14)	Co(1)-O(2)	2.1407(13)	Co(1)-N(1)	2.1442(15)
Co(1)-O(4)#2	2.0390(13)	Co(1)-N(6)#3	2.1408(16)	Co(1)-O(1)	2.2069(15)
N(6)-Co(1)#4	2.1408(16)	O(3)-Co(1)#1	2.0231(14)	O(2)-Co(1)-O(1)	60.05(5)
O(4)#2-Co(1)-N(6)#3	92.14(6)	N(6)#3-Co(1)-N(1)	177.02(7)	N(1)-Co(1)-O(1)	88.78(6)
O(2)-Co(1)-N(6)#3	88.49(6)	O(3)#1-Co(1)-O(1)	153.37(5)	O(4)#2-Co(1)-O(1)	99.04(5)
O(3)#1-Co(1)-N(1)	92.91(6)	O(3)#1-Co(1)-O(4)#2	107.59(6)	O(4)-Co(1)#5	2.0391(13)
O(4)#2-Co(1)-O(2)	159.09(6)	O(4)#2-Co(1)-N(1)	85.39(6)	N(6)#3-Co(1)-O(1)	89.96(6)
O(3)#1-Co(1)-N(6)#3	89.43(6)	O(2)-Co(1)-N(1)	93.21(6)		
2					
Co(1)-O(2)#1	2.0225(1)	Co(1)-O(1)	2.0537(14)	Co(1)-N(1)	2.1454(18)
Co(1)-O(3)#3	2.1806(15)	Co(1)-N(4)#2	2.1404(17)	Co(1)-C(26)#3	2.515(2)
Co(1)-O(4)#3	2.1958(15)	O(1)-Co(1)-N(1)	92.32(7)	O(2)#1-Co(1)-O(3)#3	97.23(6)
O(2)#1-Co(1)-C(26)#3	127.23(6)	O(1)-Co(1)-C(26)#3	128.58(6)	N(4)#2-Co(1)-C(26)#3	92.09(7)
N(1)-Co(1)-C(26)#3	87.17(7)	O(1)-Co(1)-O(3)#3	158.56(6)	N(4)#2-Co(1)-O(3)#3	92.82(7)
O(1)-Co(1)-O(4)#3	98.66(6)	O(2)#1-Co(1)-O(4)#3	157.08(6)	N(1)-Co(1)-O(3)#3	88.09(7)
O(4)#3-Co(1)-C(26)#3	29.96(6)	N(4)#2-Co(1)-O(4)#3	88.12(7)	N(1)-Co(1)-O(4)#3	89.69(7)
O(2)#1-Co(1)-O(1)	104.19(6)	O(3)#3-Co(1)-O(4)#3	59.90(5)	O(2)#1-Co(1)-C(26)#3	127.23(6)
N(1)-Co(1)-C(26)#3	87.17(7)	O(1)-Co(1)-C(26)#3	128.58(6)	N(4)#2-Co(1)-C(26)#3	92.09(7)
O(2)#1-Co(1)-N(4)#2	91.77(7)	O(1)-Co(1)-N(4)#2	85.71(6)	O(2)#1-Co(1)-N(1)	91.16(7)
O(3)#3-Co(1)-C(26)#3	30.01(6)	N(4)#2-Co(1)-N(1)	176.80(7)	O(1)-Co(1)-N(1)	92.32(7)
3					
O(2)-Co(1)-O(1)	60.33(13)	Co(1)-O(4)#1	2.0225(1)	Co(1)-N(5)#2	2.144(4)
Co(1)-N(1)	2.152(4)	Co(1)-O(5)	2.079(4)	Co(1)-O(1)	2.182(3)
Co(1)-O(2)	2.153(4)	O(4)#1-Co(1)-N(5)#2	93.44(13)	O(5)-Co(1)-N(5)#2	89.11(14)
N(1)-Co(1)-O(1)	89.49(13)	N(5)#2-Co(1)-O(1)	90.10(13)	N(5)#2-Co(1)-O(2)	94.85(14)
O(5)-Co(1)-O(2)	162.54(13)	O(4)#1-Co(1)-O(2)	102.27(14)	N(5)#2-Co(1)-N(1)	176.84(15)
O(5)-Co(1)-N(1)	87.93(14)	O(4)#1-Co(1)-N(1)	87.89(14)	O(4)-Co(1)#3	2.020(3)
O(5)-Co(1)-O(1)	102.75(14)	O(4)#1-Co(1)-O(1)	162.50(13)	N(1)-Co(1)-O(2)	87.67(14)
O(4)#1-Co(1)-O(5)	94.44(14)				

[a] Symmetry transformations used to generate equivalent atoms: **For 1**: #1 -*x*, -*y* + 1, -*z* + 1 #2 *x* + 1, *y*, *z* #3 *x*, *y* + 1, *z* + 1 #4 *x*, *y* - 1, *z* - 1 #5 *x* – 1, *y*, *z;* For **2**: #1 -*x* + 2, -*y* + 1, -*z* + 1 #2 *x* + 1, *y* + 1, *z* + 1 #3 *x* - 1, *y*, *z* #4 *x* + 1, *y*, *z* #5 *x* - 1, *y* - 1, *z* - 1; For **3**: #1 *x* - 1, *y*, *z* #2 *x*, *y*, *z* - 1 #3 *x* +1, *y*, *z* #4 *x* , *y*, *z* + 1 #5 -*x* -1, -*y* + 1, -*z* + 1.

Table S3. *SHAPE* analysis of Co1 ion in MOF **1**.

Label	**Shape**	**Symmetry**	**Distortion**
HP-6	Hexagon	D_{6h}	30.605
PPY-6	Pentagonal pyramid	C_{5v}	23.401
OC-6	Octahedron	O_h	2.303
TPR-6	Trigonal prism	D_{3h}	12.165
JPPY-6	Johnson pentagonal pyramid J2	C_{5v}	27.341

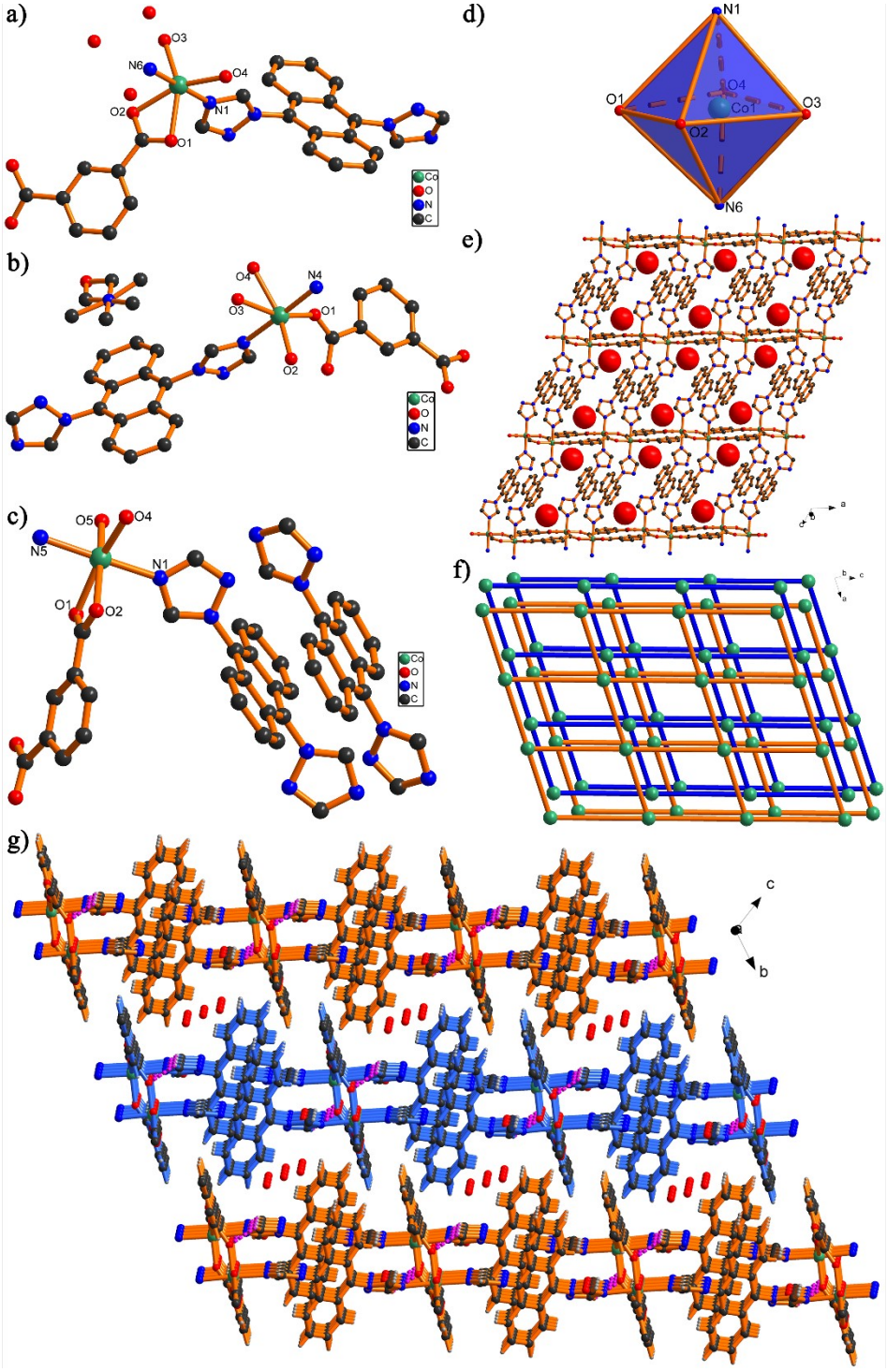

Fig. S1 The asymmetric units of MOF **1** (a), **2** (b) and **3** (c), H atoms are omitted for clarity; d) The coordination geometry of Co1 ion in MOF **1**; e) The 2D layer of MOF **1**; f) The 4-connected '**sql**'-type topology of MOF **1**; g) The 3D supramolecular structure of MOF **1**. (hydrogen bonding interactions are denoted by purple dot lines.)

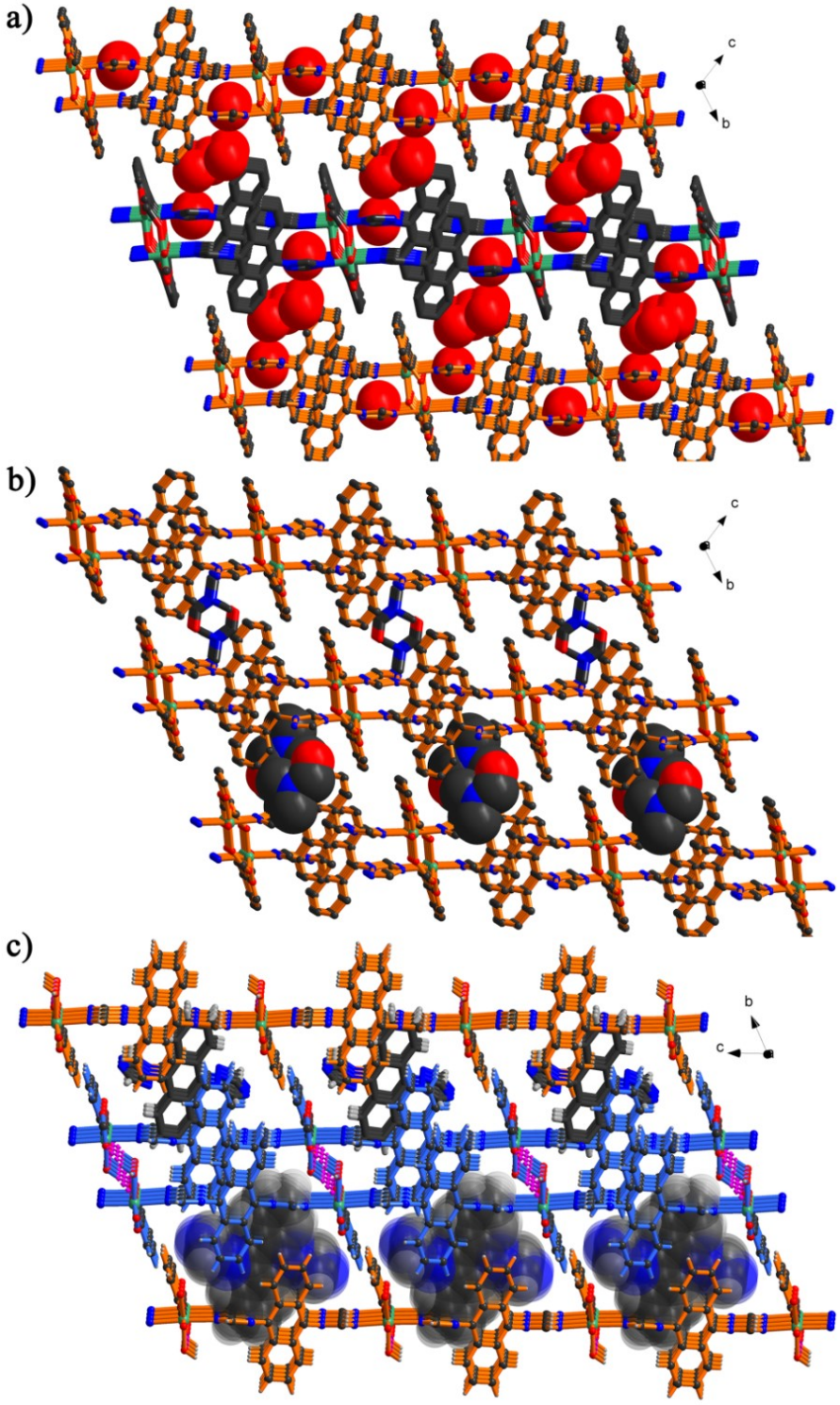

Fig. S2 The 3D supramolecular structures of MOFs **1** (a), **2** (b) and **3** (c).

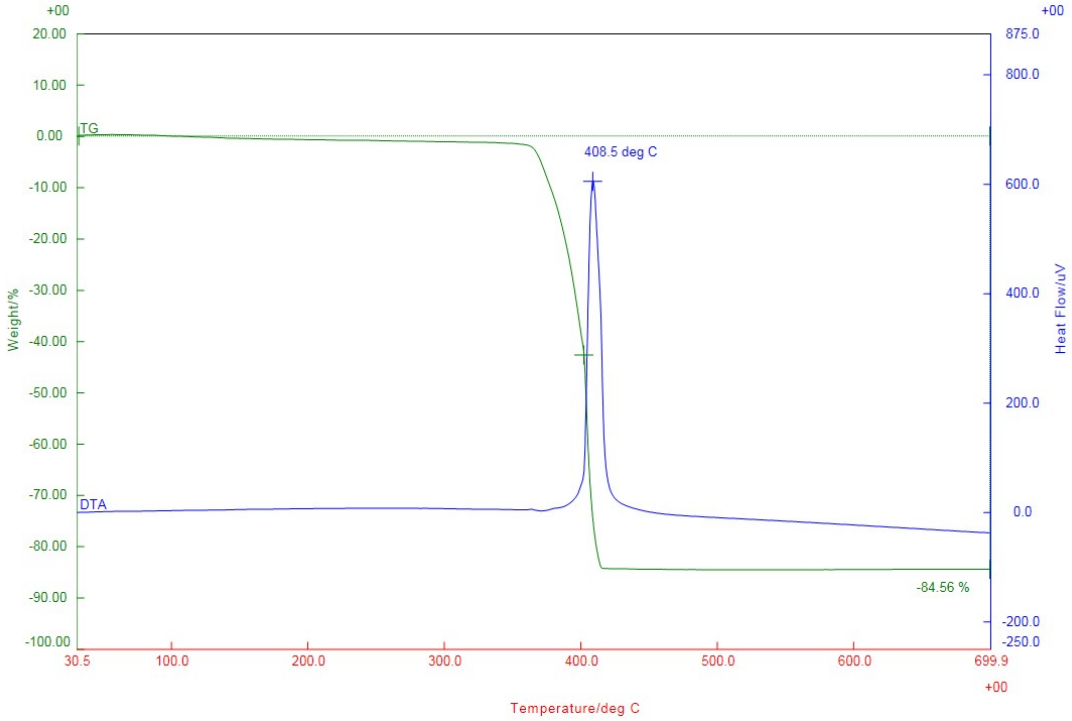

Fig. S3 TGA plot of MOF **1**.

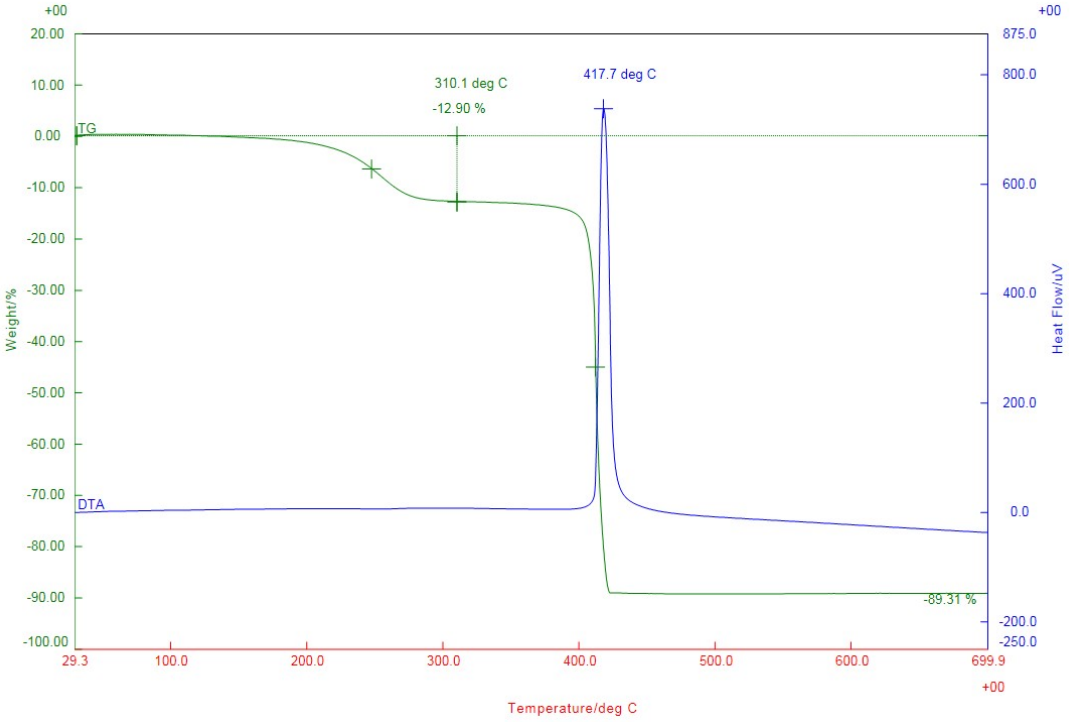

Fig. S4 TGA plot of MOF **2**.

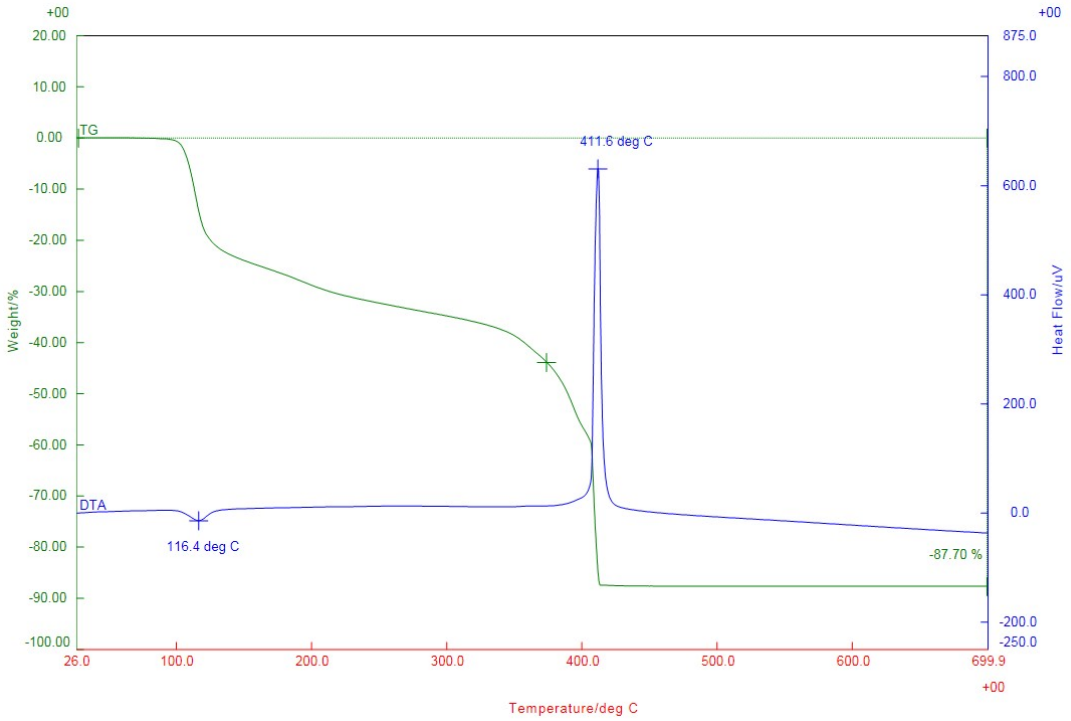

Fig. S5 TGA plot of MOF **3**.

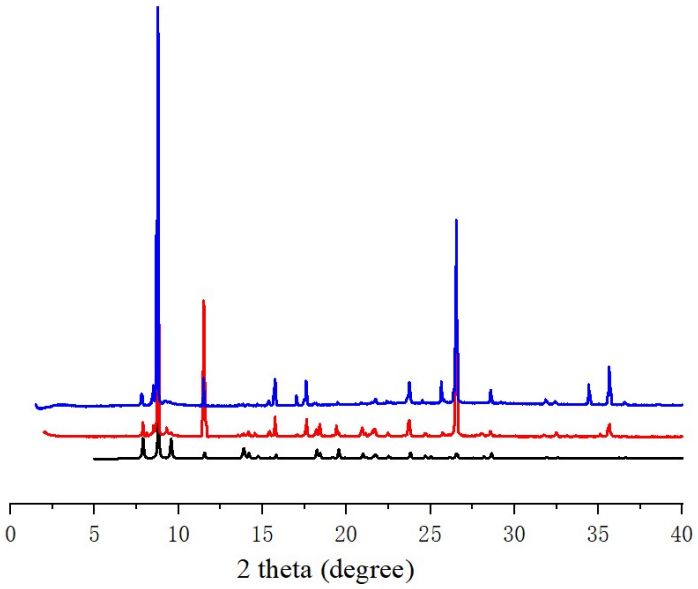

Fig. S6 PXRD patterns of MOF **1**. Black, simulated; red, as-synthesized; blue, active sample of MOF **1** before N_2 adsorption.

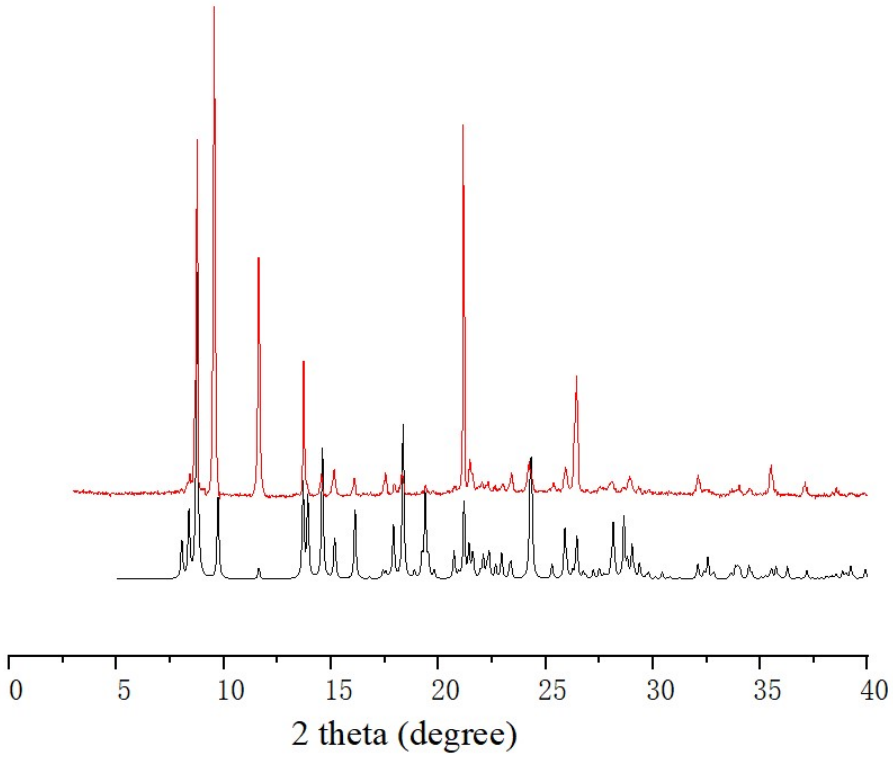

Fig. S7 PXRD patterns of MOF **2**. Black, simulated; red, as-synthesized.

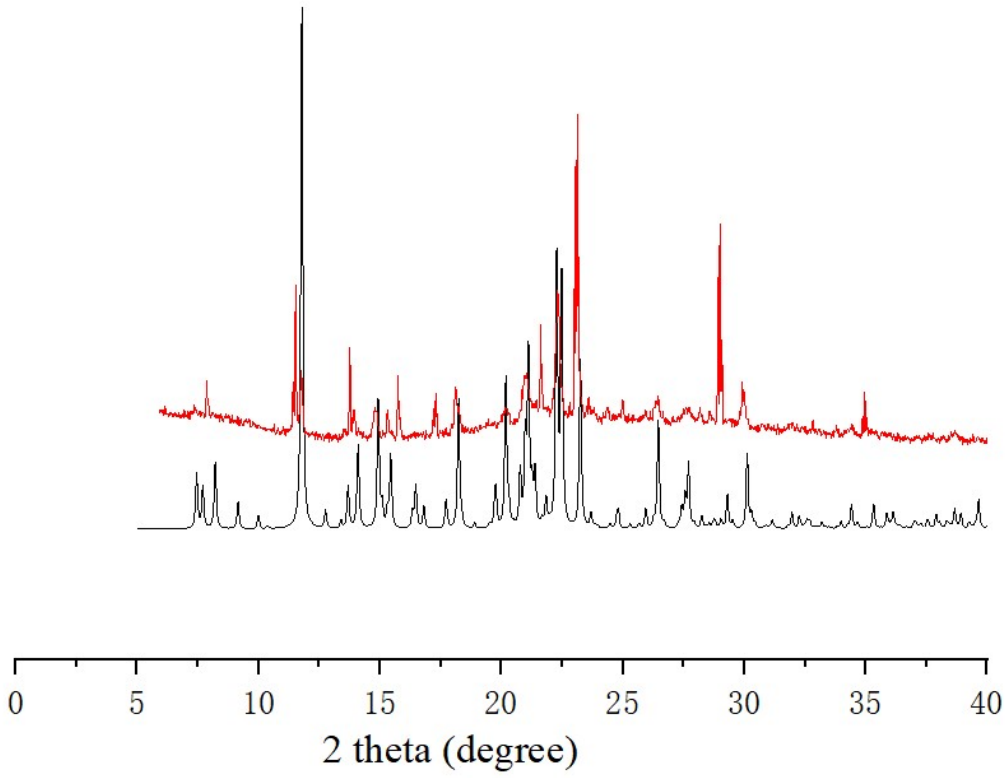

Fig. S8 PXRD patterns of MOF **3**. Black, simulated; red, as-synthesized.

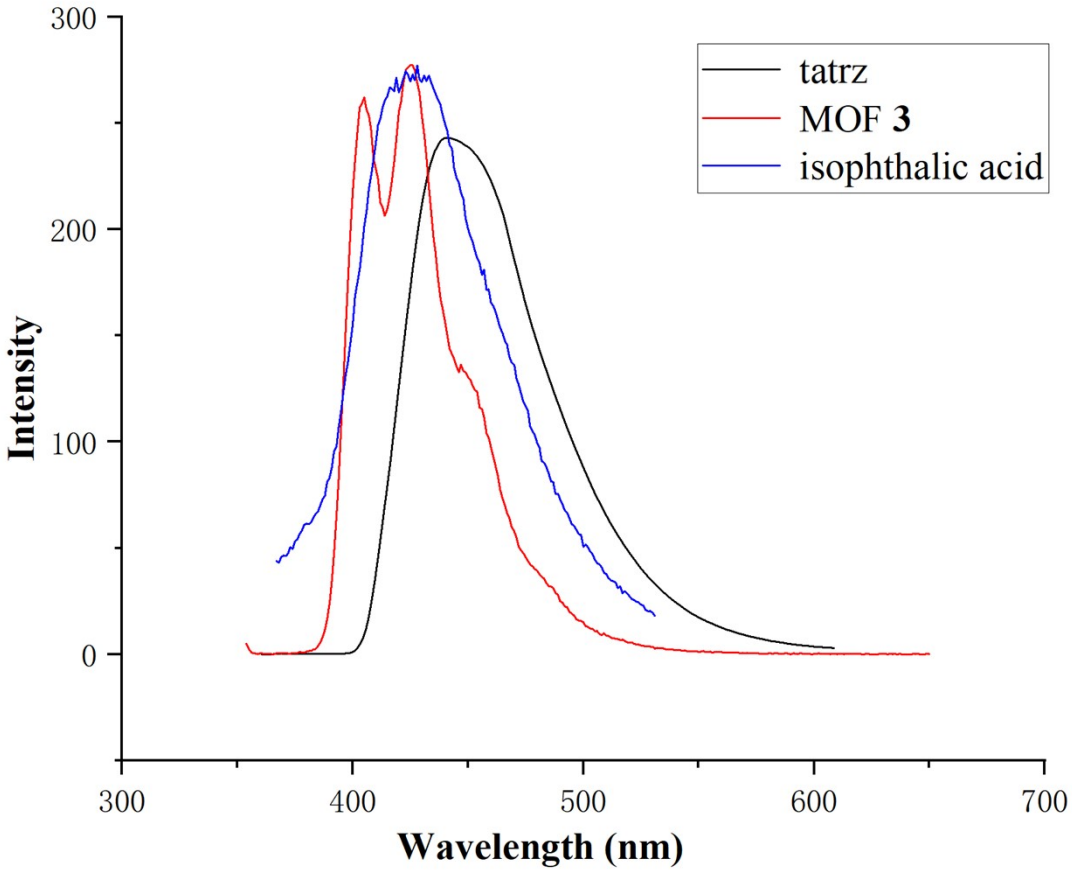

Fig. S9 Emission spectra of tatrz, MOF **3** and isophthalic acid in DMF solution at room temperature which are excited at 343 nm. Black, tatrz; red, MOF **3**, blue, isophthalic acid.

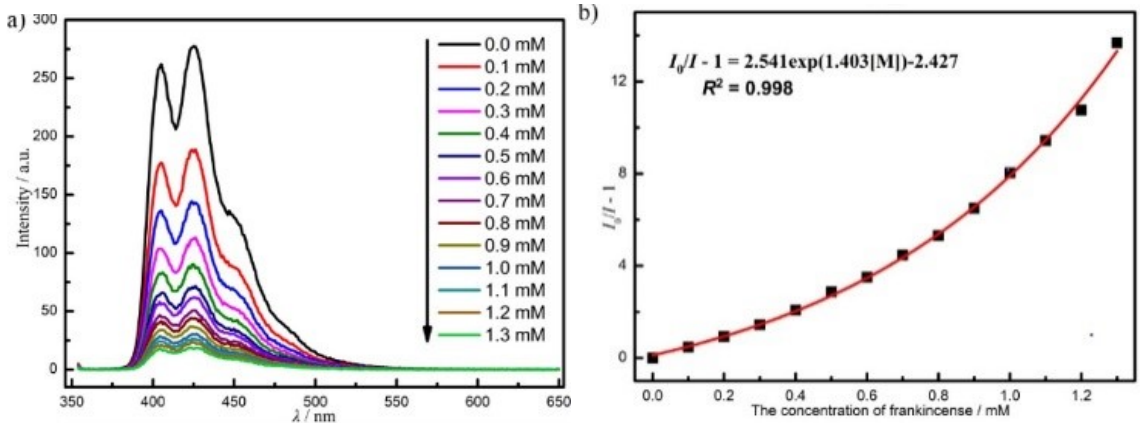

Fig. S10 (a) The concentrations-dependent luminescence spectra of **3** towards frankincense; (b) the fitting curve of the nonlinear S-V plots of **3** for various concentrations of frankincense by the exponential quenching equation.

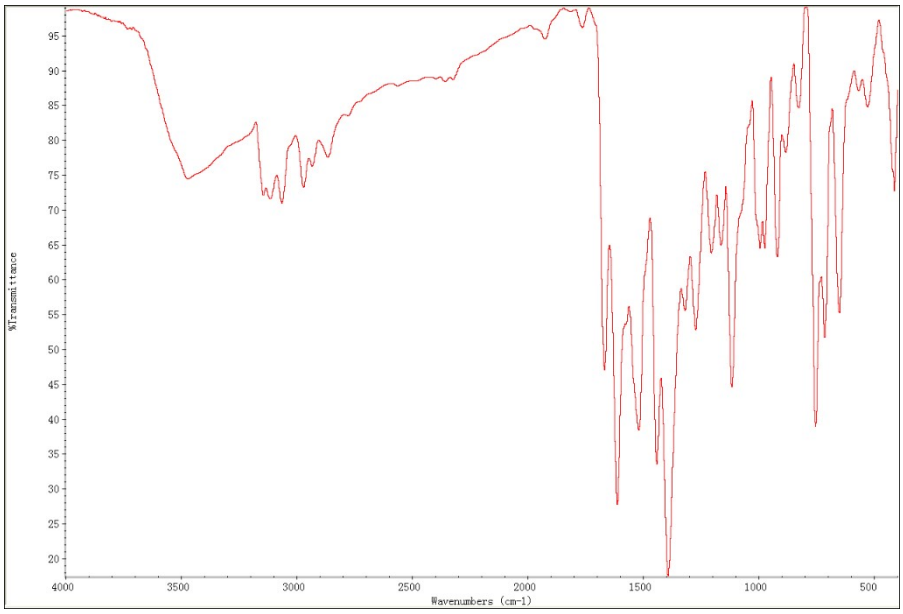

Fig. S11 FT-IR spectrum of MOF **1**.

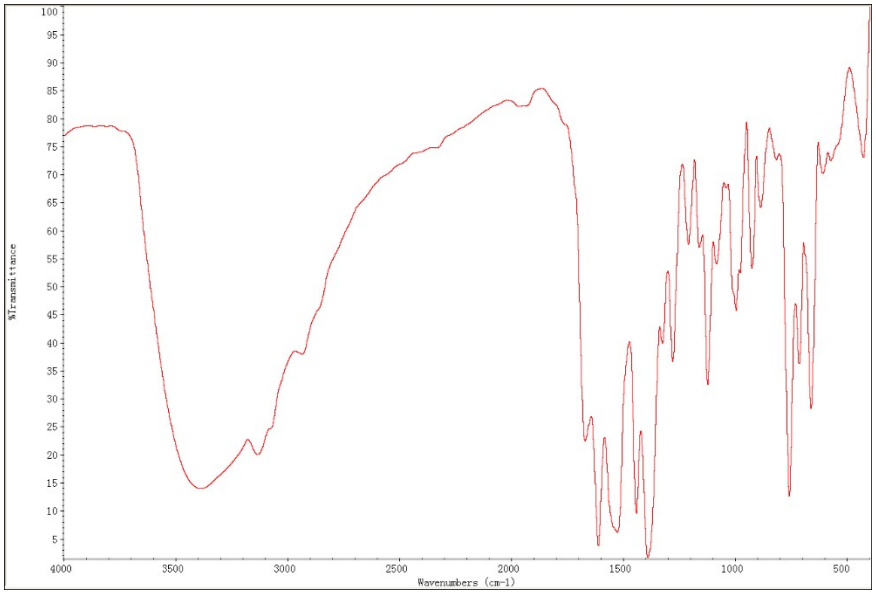

Fig. S12 FT-IR spectrum of MOF **2**.

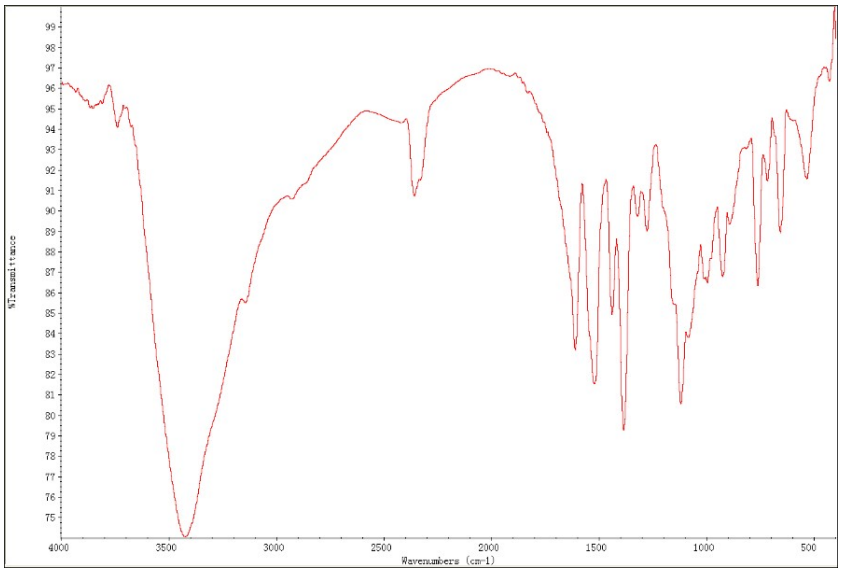

Fig. S13 FTIR spectrum of MOF **3**.

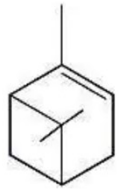

α-pinene (the main component of frankincense)

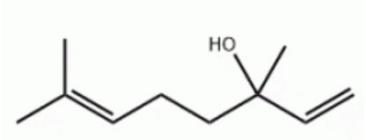

linalool (the main component of lanvender)

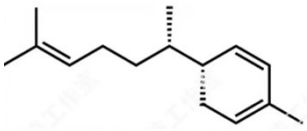

α-zingiberene (the main component of ginger)

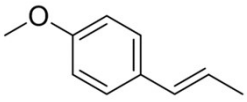

anisene (the main component of fennel)

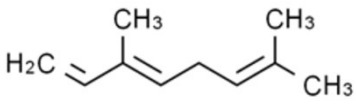

ocimene (the main component of basil)

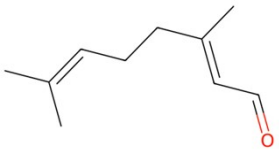

citral (the main component of lemongrass)

Fig. S14 The constitutional formula of the main component of frankincense, lanvender, ginger, fennel, basil, and lemongrass.

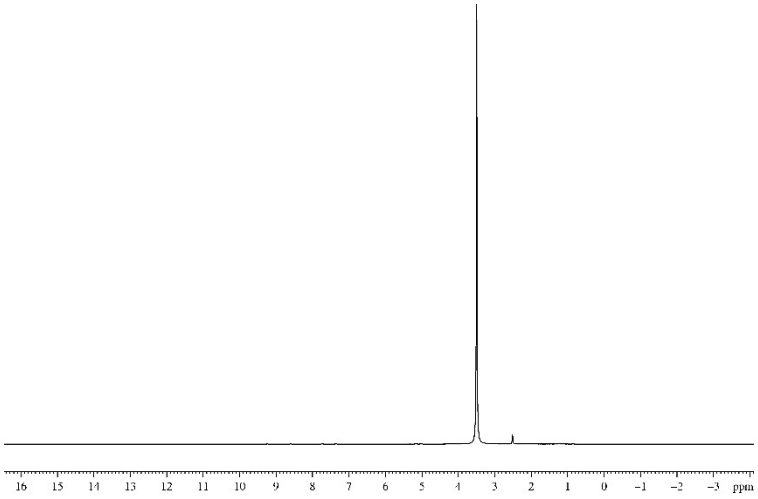

Fig. S15 ^{1}H NMR spectrum (400 mHz) of MOF **3** in DMSO-d_6 at 25 ^{o}C.

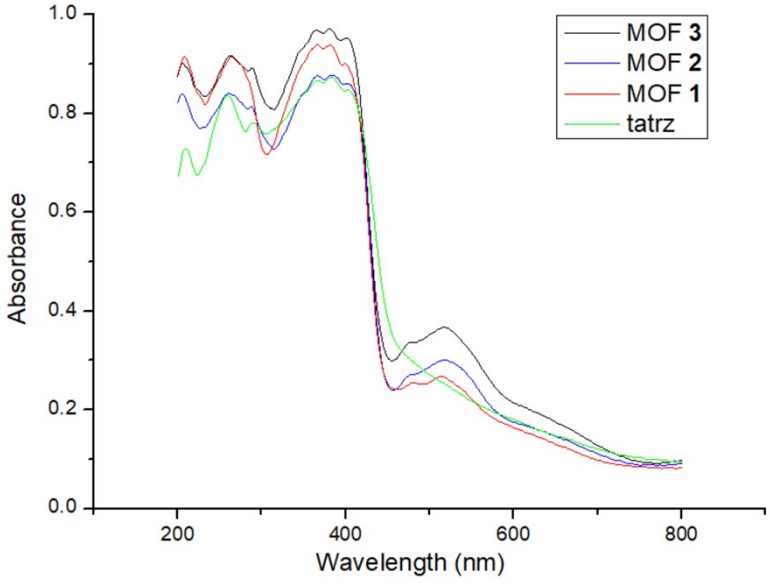

Fig. S16 Solid UV-vis absorption spectra for MOF **1**-**3** at room temperature.

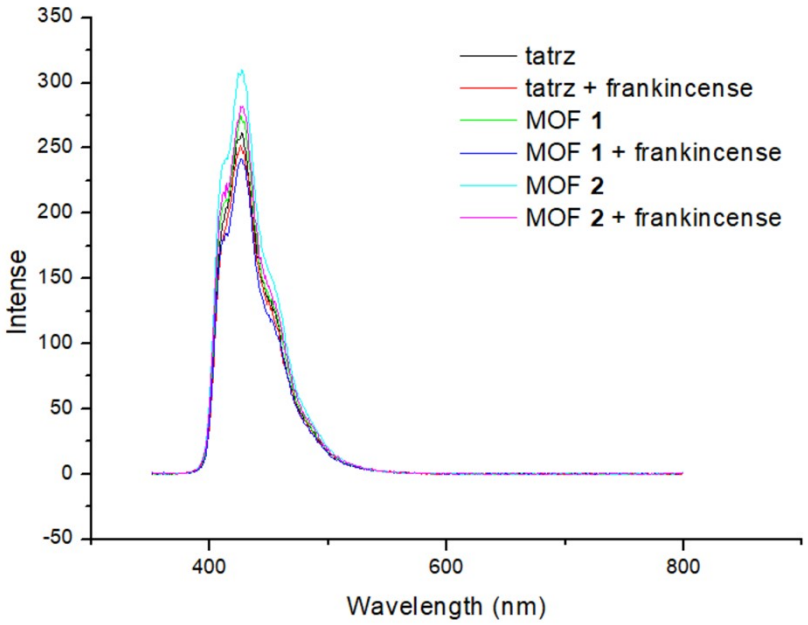

Fig. S17. Emission spectra of tatrz, tatrz added frankincense, MOF **1**, MOF **1** added frankincense, MOF **2**, MOF **2** added frankincense in DMF solution at room temperature which are excited at 343 nm.

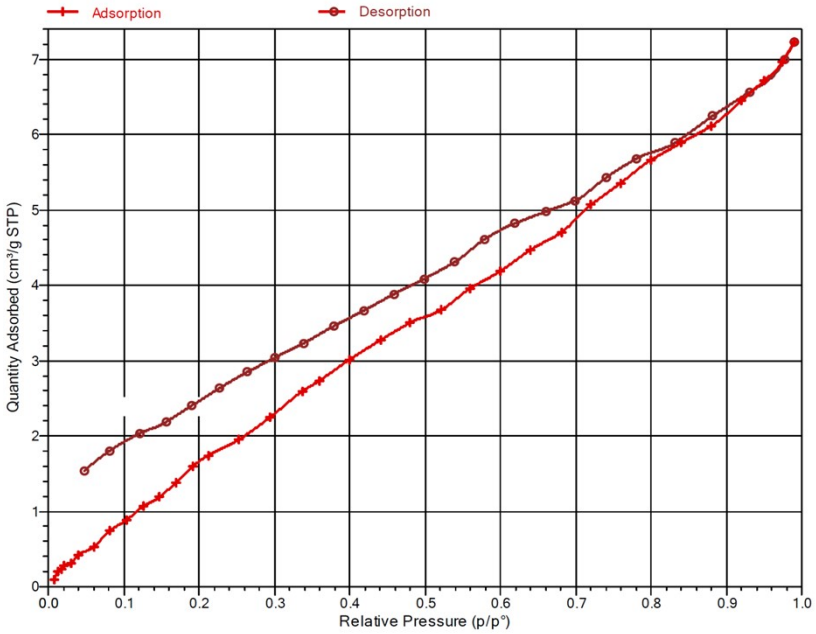

Fig. S18. N_2 adsorption isotherms of MOF **3** sheets at 1 bar, 77 K.

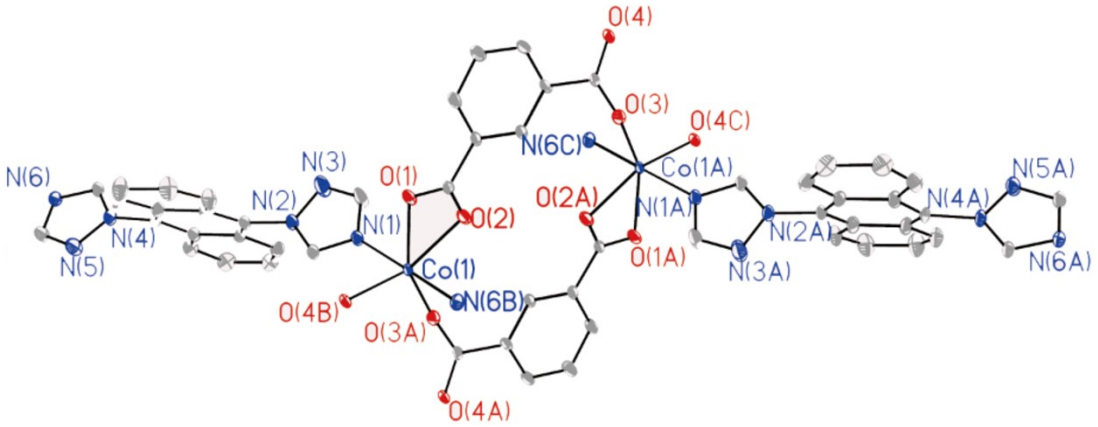

Fig. S19. ORTEP drawing with an atomic labeling system of MOF **1**.

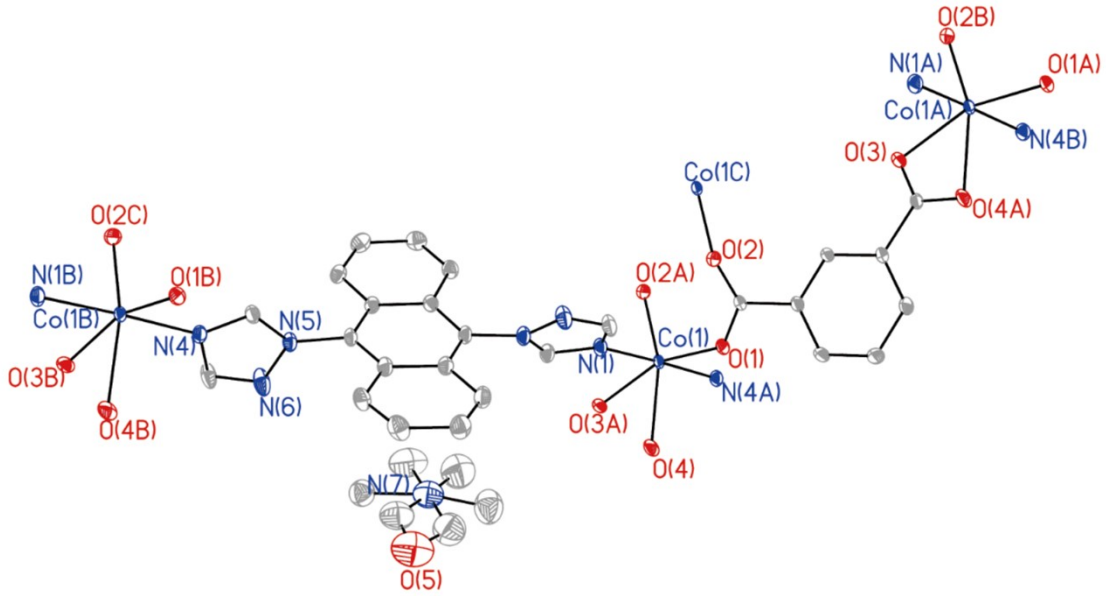

Fig. S20. ORTEP drawing with an atomic labeling system of MOF **2**.

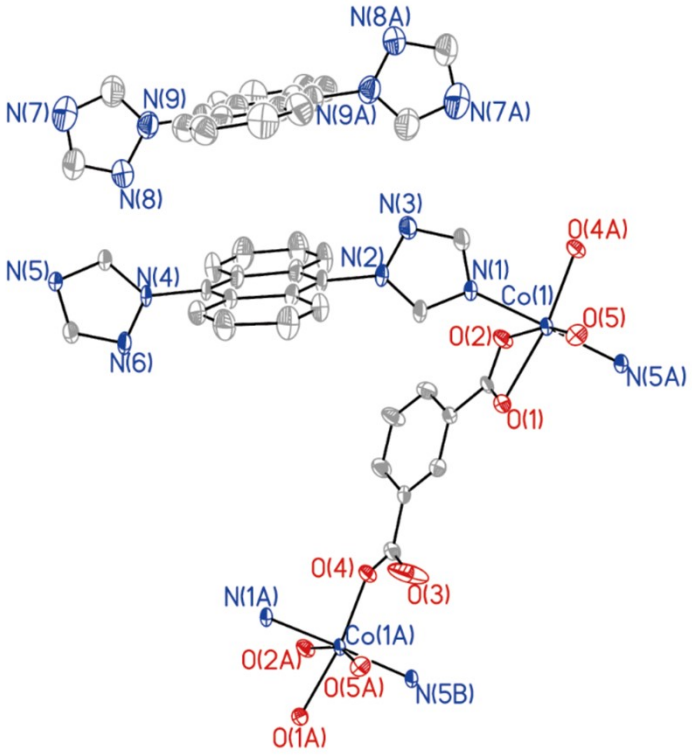

Fig. S21. ORTEP drawing with an atomic labeling system of MOF **3**.

(a)

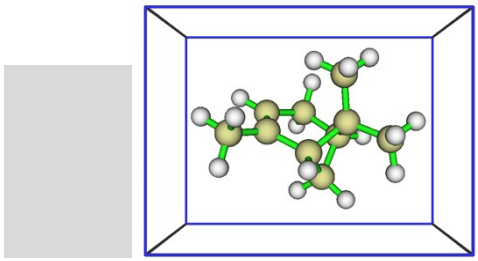

α-pinene (main component of frankincense)

```
size
 Farthest distance:   21(H )  ---   24(H ):     6.747 Angstrom
 vdW radius of   21(H ): 1.200 Angstrom
 vdW radius of   24(H ): 1.200 Angstrom
 Diameter of the system:     9.147 Angstrom
 Radius of the system:     4.574 Angstrom
 Length of the three sides:     9.131     7.429     6.961 Angstrom
```

(b)

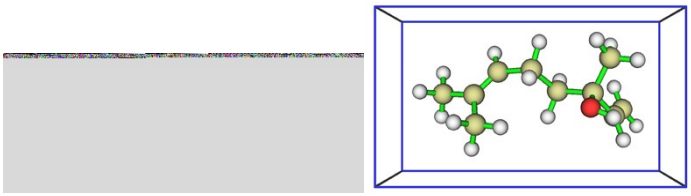

linalool (main component of lanvender)

```
size
 Farthest distance:   12(H )  ---   24(H ):     9.250 Angstrom
 vdW radius of   12(H ): 1.200 Angstrom
 vdW radius of   24(H ): 1.200 Angstrom
 Diameter of the system:    11.650 Angstrom
 Radius of the system:     5.825 Angstrom
 Length of the three sides:    11.299     6.571     6.607 Angstrom
```

(c)

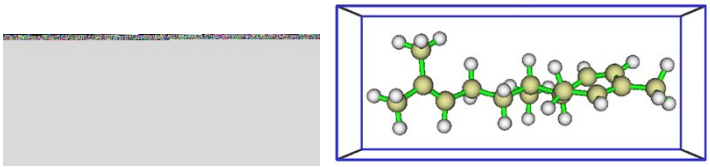

α-zingiberene (main component of ginger)

```
size
 Farthest distance:   11(H )  ---   39(H ):    12.611 Angstrom
 vdW radius of   11(H ): 1.200 Angstrom
 vdW radius of   39(H ): 1.200 Angstrom
 Diameter of the system:    15.011 Angstrom
 Radius of the system:     7.505 Angstrom
 Length of the three sides:    15.003     8.198     6.220 Angstrom
```

(d)

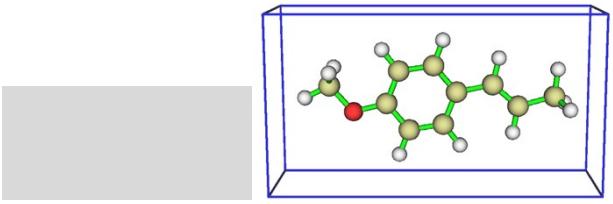

anisene (main component of fennel)

```
size
 Farthest distance:   12(H )  ---   22(H ):    10.529 Angstrom
 vdW radius of   12(H ): 1.200 Angstrom
 vdW radius of   22(H ): 1.200 Angstrom
 Diameter of the system:    12.929 Angstrom
 Radius of the system:     6.465 Angstrom
 Length of the three sides:    12.887     7.027     4.189 Angstrom
```

(e)

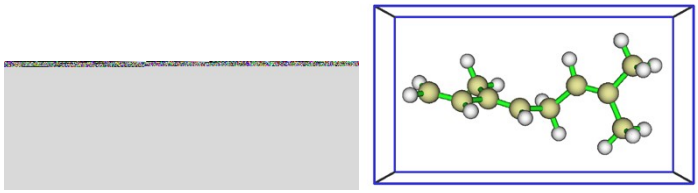

ocimene (main component of basil)

```
size
 Farthest distance:   11(H )  ---   21(H ):     9.802 Angstrom
 vdW radius of   11(H ): 1.200 Angstrom
 vdW radius of   21(H ): 1.200 Angstrom
 Diameter of the system:    12.202 Angstrom
 Radius of the system:     6.101 Angstrom
 Length of the three sides:    11.968     6.516     6.635 Angstrom
```

(f)

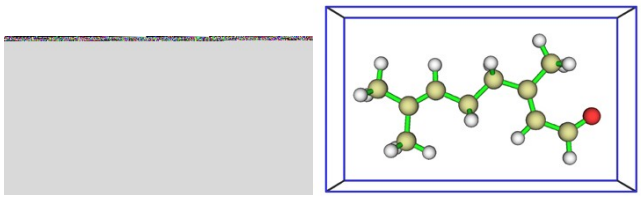

citral (main component of lemongrass)

```
size
 Farthest distance:   11(O )  ---   14(H ):     9.842 Angstrom
 vdW radius of   11(O ): 1.520 Angstrom
 vdW radius of   14(H ): 1.200 Angstrom
 Diameter of the system:    12.562 Angstrom
 Radius of the system:     6.281 Angstrom
 Length of the three sides:    12.481     7.419     4.161 Angstrom
```

Fig. S22. The six structures opt b3lyp 6-31g(d) were optimized using Gauss and the sizes of the six molecules were calculated using multiwfn.